

---

# A scattering study of nucleation phenomena in polymer crystallisation

---

Anthony J. Ryan,<sup>\*ab</sup> J. Patrick A. Fairclough,<sup>a</sup> Nicholas J. Terrill,<sup>b</sup> Peter D. Olmsted<sup>c</sup> and Wilson C. K. Poon<sup>d</sup>

<sup>a</sup> Department of Chemistry, The University of Sheffield, Sheffield, UK S3 7HF

<sup>b</sup> CCLRC Daresbury Laboratory, Warrington, UK WA4 4AD

<sup>c</sup> Department of Physics, The University of Leeds, Leeds, UK LS 9JT

<sup>d</sup> Department of Physics and Astronomy, The University of Edinburgh, Edinburgh, UK EH9 3JZ

Received 7th January 1999

The mechanism of primary nucleation in polymer crystallisation has been investigated experimentally and theoretically. Two types of experiments have been performed on polypropylene, polyethylene, and poly(ethylene terephthalate). Crystallisations with long induction times, studied by small and wide angle X-ray scattering (SAXS and WAXS), reveal the onset of large scale ordering prior to crystal growth. Rapid crystallisations studied by melt extrusion indicate the development of well resolved oriented SAXS patterns associated with large scale order before the development of crystalline peaks in the WAXS region. The results suggest pre-nucleation density fluctuations play an integral role in polymer crystallisation. A theoretical model has been developed which qualitatively describes the experimental results.

---

## Introduction

Processing of semicrystalline thermoplastics relies on the shaping of molten material in either moulds or dies and the stabilisation of the shape produced by crystallisation.<sup>1</sup> During crystallisation a microstructure develops which can control the mechanical and aesthetic properties of the polymer. To produce useful materials it is essential to understand and predict this process.

Polymers in solutions and melts can be regarded as random objects whose size and shape is governed by inter- and intra-molecular interactions but is dominated by entropy. In the crystal this is no longer true and the behaviour of the chain is now influenced by the proximity of the neighbouring chains and the van de Waals forces which act between them. The Gibbs free energy,  $G$ , is a balance between entropy,  $S$ , and the enthalpy,  $H = U + pV$ , where  $U$  is the internal energy,  $p$  the pressure and  $V$  the volume of the system, thus

$$G(T, p) = (U + pV) - TS \quad (1)$$

In the melt, entropy dominates and the polymer has a Gaussian (random) structure. Crystallisation is a process involving the regular arrangement of chains and is consequently associated with a large negative entropy change. For the free energy change upon crystallisation to be

favourable there must also be a large negative enthalpy change, generally associated with an increase in density and a reduction in internal energy

The creation of a stable 3-D structure from a disordered state (*i.e.* a polymer melt) is generally considered a two step process. The first step is called *nucleation* and involves the creation of a stable nucleus from the entangled polymer melt. Most technical processes involve secondary or heterogeneous nucleation either from specially added surfaces, nucleating agents, or adventitious surfaces, such as dust particles.

In primary (homogeneous) nucleation, creation of a stable nucleus is brought about by the ordering of chains in a parallel array stimulated by intermolecular forces. As a melt is cooled there is a tendency for the molecules to move toward their lowest energy conformation, and this will favour the formation of co-operatively ordered chains and thus nuclei. However two factors impede the ordering required for nucleation; cooling, which reduces diffusion coefficients, and chain entanglements. In fact the thermal motion needed for diffusion may be enough to cause the incipient nuclei to melt. The second step is growth of the crystalline region by the addition of other chain segments to the nucleus. This growth is impeded by low diffusion coefficients at low temperatures and thermal redispersion of the chains at the crystal/melt interface at high temperatures. Thus, the crystallisation process is limited to a range of temperatures between the glass transition temperature,  $T_g$  and the melting point,  $T_m$ . The alignment of polymer chains at specific distances from one another to form crystalline nuclei will be favoured when intermolecular forces are strong. The greater the interaction between chains and the easier they can pack the greater the energy change will be. Thus symmetrical chains and strongly interacting chains are more likely to form stable crystals.

Despite the maturity and market penetration of the polymer industry one aspect of polymer processing, *primary nucleation*, is little understood. Whereas the growth of polymer crystals is well established in literature, and there are usable theories to predict the kinetics of crystallisation, understanding of the initiation or nucleation step remains somewhat of a mystery. The available theories are complicated and somewhat unphysical.<sup>2</sup> There is good reason for this, experimental access to the nucleation step is very difficult whereas studies of crystal growth are simple enough to be used in undergraduate laboratory classes.<sup>3</sup>

Upon cooling a crystallisable polymer melt a hierarchy of ordered structures emerges. Elegant experimental and theoretical work (on melt and solution crystallised materials, especially single crystals) in the 1960s and 70s allowed useful models to be developed.<sup>4,5</sup> First there are crystalline 'lamellae', comprising regularly packed polymer chains, each of which is ordered into a specific helical conformation. These lamellae interleave with amorphous layers to form 'sheaves', which in turn organise to form superstructures, *e.g.* spherulites. These structures may be probed by various techniques: wide-angle X-ray scattering (WAXS) is sensitive to atomic order within lamellae (giving rise to Bragg peaks), while small-angle X-ray scattering (SAXS) probes lamellae and their stacking. Electron microscopy is useful for visualising the crystal structure (by selected area electron diffraction), the lamellae morphology (by transmission microscopy of surface replicas, or direct scanning electron microscopy) and spherulites (by scanning electron microscopy) and this has been reviewed in some detail.<sup>6</sup> The growth of crystals by secondary nucleation have been explained by various versions of "regime" theories.<sup>2</sup>

In the classical picture of polymer melt crystallisation we expect and observe Bragg peaks in WAXS after an induction period  $\tau_i$ . SAXS accompanies the WAXS, corresponding to interleaved crystal lamellae and amorphous regions.<sup>7</sup> No SAXS is expected during  $\tau_i$ . However, recent experiments<sup>8-12</sup> have reported SAXS peaks during the induction period and before the emergence of Bragg peaks. Initially the SAXS peak intensity grows exponentially, and it may be reasonably fitted to Cahn-Hilliard (CH) theory<sup>13</sup> for spinodal decomposition; that is the spontaneous growth of fluctuations indicative of thermodynamic instability. The peak moves to smaller angles in time, stopping when Bragg peaks emerge. By fitting to CH theory an extrapolated spinodal temperature (at which the melt first becomes unstable towards local density fluctuations) can be obtained.<sup>12</sup> Spinodal kinetics have been reported in different polymer melts: poly(ethylene terephthalate) (PET),<sup>8-10</sup> poly(ether ketone ketone) (PEKK),<sup>11</sup> polyethylene (PE) and isotactic polypropylene (iPP).<sup>12</sup> An argument has been made against the spinodal crystallisation mode, by Janeschitz-Kriegl,<sup>14</sup> who invoked a variety of liquid-gas analogies and consideration of surface tensions, in spite of considerable experimental evidence for spinodal modes. To explain recent results, a spino-

dally assisted crystallisation (SAC) model has been developed,<sup>15</sup> which deals with the contributions to the free-energy in terms of coupled order parameters of density and chain conformation and predicts a liquid–liquid phase diagram buried in the liquid–crystal coexistence region.

Recent rheological studies<sup>16</sup> show that gelation occurs in crystallising melts at very low degrees of crystallinity, typically <3%, shortly after  $\tau_i$ . This means that there is a percolating network formed that is observed in the dynamic mechanical response of the system. This is not consistent with impingement of spherulites which only occurs at much higher (typically >40%) degrees of crystallinity. Furthermore, there are also anomalies in the measurements of spherulite growth rates,<sup>17</sup> whilst heat capacity, volume change and X-ray experiments observe an induction time, a plot of the variation in spherulite radius with time is seen to pass through the origin, indicating that spherulites started to grow without an induction period being observed. Both pieces of evidence indicate that large-scale structure is formed prior to the appearance of Bragg peaks or evolution of appreciable enthalpy.

In this paper we present new experimental evidence for precrystallisation density fluctuations in a range of polymer melts. In order to separate nucleation from growth, two types of experiments have been performed on polypropylene, polyethylene, and poly(ethylene terephthalate). Rapid crystallisations studied by melt extrusion indicate the development of well resolved oriented SAXS patterns associated with large scale order before the development of crystalline peaks in the WAXS region. Crystallisations with long induction times, studied by small and wide angle X-ray scattering (SAXS and WAXS), reveal the onset of large scale ordering prior to crystal growth. The experiments are compared to the SAC model and discussed in light of other experimental evidence for large scale structure prior to formation of crystals with Bragg peaks.

## Experimental

### Materials

The polypropylene used was a commercial grade, S-30-S (DSM), which was free from any additives. The number-average molar mass (GPC) and the polydispersity were  $52 \text{ kg mol}^{-1}$  and 2, respectively, and the melting point (DSC) was  $165 \pm 2^\circ\text{C}$ . The as-received iPP pellets had a degree of crystallinity of 0.6 as determined from measurements of the heat of fusion. The HDPE was a commercial extrusion grade (Shell), which was free from any additives. The melting point (DSC) was  $135 \pm 2^\circ\text{C}$ .<sup>18</sup> The PET was a gift from ICI and was an experimental grade which was free from any additives. The melting point (DSC) was  $265 \pm 2^\circ\text{C}$ .<sup>18</sup>

### Fast crystallisations by SAXS/WAXS/extrusion

Simultaneous SAXS/WAXS/extrusion measurements were made on beamline 16.1 of the SRS at the CCLRC Daresbury Laboratory, Warrington, UK. The details of the storage ring, radiation and camera geometry and data collection electronics have been given in detail elsewhere.<sup>18</sup> An extruder above the X-ray position was used to provide a steady stream of crystallising polymer past the X-ray beam. Tape extrusion is a steady-state process which shows post-die plug flow, therefore the distance down the spinline where the observation was made correlates with the time since the material left the extruder die. The material in the X-ray beam is continuously replaced by material with the same shear and temperature history. A tape of polymer melt was extruded from a die (of dimensions  $0.5 \times 3 \text{ mm}$  at  $T_m + 40^\circ\text{C}$ ) and collected *via* a wind up mechanism below the X-ray beam. The extruder used was an AXON BX18 which operated in starve-feed mode to minimise the time the polymer spent in the melt. The experimental set-up is shown schematically in Fig. 1. The distance from the die head to the beam could be varied between 0.3 and 1.8 m. The camera is equipped with a multiwire area detector (SAXS) located between 3 and 8 m from the sample position with flight path between the WAXS and SAXS detector being under vacuum. Two types of area detector were employed for the WAXS. In order to observe the development of structure during an extrusion experiment a second multiwire area detector was used which was offset from the centre line of the beam and located approximately 20 cm from the extruded tape. Time resolved SAXS/WAXS measurements were made with the multiwire area detector intersecting either the meridian or the equator. The spatial resolution of the electronic area detectors is  $400 \mu\text{m}$  and they can handle up to  $\sim 500\,000 \text{ counts s}^{-1}$ . To probe a wide range of reciprocal

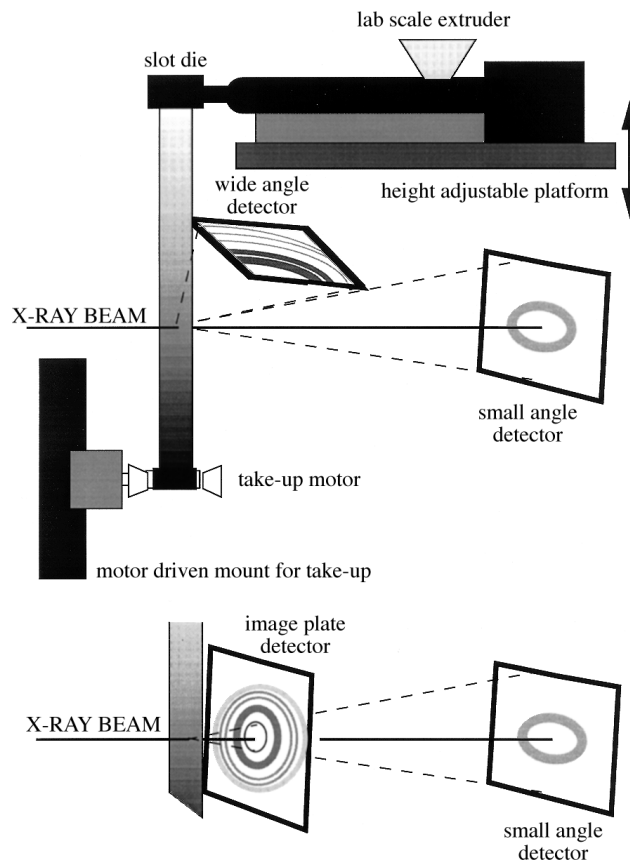


Fig. 1 Schematic diagram of the SAXS/WAXS/extrusion experimental set-up.

space an image plate with a hole was used to record flat plate WAXS patterns contemporaneously with SAXS. The exposure time was set at 30 s using a mechanical shutter. A4 size Fuji and Kodak image plates were read with a Molecular Dynamics image plate reader with a spatial resolution of 176  $\mu\text{m}$ .

The scattering pattern from an oriented specimen of wet collagen (rat-tail tendon) was used to calibrate the SAXS detector and HDPE, aluminium and an NBS silicon standard were used to calibrate the WAXS detectors.<sup>19</sup> Parallel-plate ionisation detectors, placed before and after the sample, recorded the incident and transmitted intensities. The experimental data were corrected for background scattering for sample thickness and transmission, and for the positional alinearity of the detectors.

#### Slow crystallisations by SAXS/WAXS/DSC

Simultaneous SAXS/WAXS/DSC measurements were made on beamline 8.2 of the SRS at the CCLRC Daresbury Laboratory, Warrington, UK. The details of the storage ring, radiation and camera geometry and data collection electronics have been given in detail elsewhere.<sup>20</sup> The camera is equipped with a multiwire quadrant detector (SAXS) located 3.5 m from the sample position and a curved knife-edge detector (WAXS) that covers 120° of arc at a radius of 0.2 m. A vacuum chamber is placed between the sample and detectors in order to reduce air scattering and absorption. The WAXS detector has a spatial resolution of 100  $\mu\text{m}$  and can monitor up to  $\sim 50\,000$  counts  $\text{s}^{-1}$ ; only 60° of arc are active in these experiments with the rest of the detector being shielded with lead. A beamstop is mounted just before the SAXS exit window to prevent the

direct beam from hitting the SAXS detector which measures intensity in the radial direction (over an opening angle of  $70^\circ$  and an active length of 0.2 m) and is suitable only for isomorphous scatterers. The spatial resolution of the SAXS detector is  $200\ \mu\text{m}$  and it can handle up to  $\sim 500\,000$  counts  $\text{s}^{-1}$ . Disk specimens of polymer (thickness  $\sim 1$  mm, diameter  $\sim 6$  mm) were cut from pre-moulded sheet. A disk specimen for SAXS/WAXS/DSC was encapsulated in a TA Instruments DSC fitted with mica windows (thickness  $\sim 25\ \mu\text{m}$ , diameter  $\sim 7$  mm), and the pan was inserted into a Linkam DSC apparatus of the single-pan design that has been described in detail elsewhere.<sup>20</sup> The cell comprises a silver furnace around a heat-flux plate containing  $3 \times 0.5$  mm slot, for X-ray access, and the sample is held in contact with the plate by a spring of low thermal mass. The temperature was calibrated using the melting points of high purity indium and tin. In the present study, a multi-stage temperature programme was used as follows: for iPP and HDPE (i) heat to  $200^\circ\text{C}$  at  $50^\circ\text{C}\ \text{min}^{-1}$ ; (ii) hold at  $200^\circ\text{C}$  for 1 min; (iii) cool at  $60^\circ\text{C}\ \text{min}^{-1}$  to the crystallisation temperature and hold for 10–120 min depending on the temperature. The PET samples were heated to  $290^\circ\text{C}$ . The crystallisation time at each temperature was chosen so that at least half primary crystallisation kinetics were observed. Data acquisition strategies were chosen so that for the longer crystallisations the samples were only exposed to the X-ray beam for 10% of the time after crystallisation had started, to limit beam damage. Data were reduced to intensity *versus* scattering vector using the CCP13 programme *xotoko*.<sup>21</sup> The peak intensities and areas were calculated using the CCP 13 programme *fit*.<sup>22</sup> For the SAXS data a Gaussian peak (whose position was a variable) was fitted on top of a Porod background. For the WAXS Gaussian peaks were fitted on top of a Gaussian background. In iPP the positions of the 4 Gaussian peaks were set according to the positions of the iPP reflections at *hkl* values of 110, 040, 130, (111, 131, 041). Two Gaussian peaks were fitted at the positions of the 110 and 200 reflections for HDPE and for 100 and 110 reflections for PET.

## Results

The crystallisation curve shown in Fig. 2 was obtained in a SAXS/WAXS/DSC experiment from iPP (ref. 23) and shows the classic features of primary crystallisation. The detailed molecular structure of the polymer, the specific nature of the nucleation process and the degree of under-cooling determine the magnitude of the lamellar thickness and the degree of crystallinity within the lamellar stacks. The crystallisation kinetics are analysed using the Avrami model,<sup>24</sup> expressed

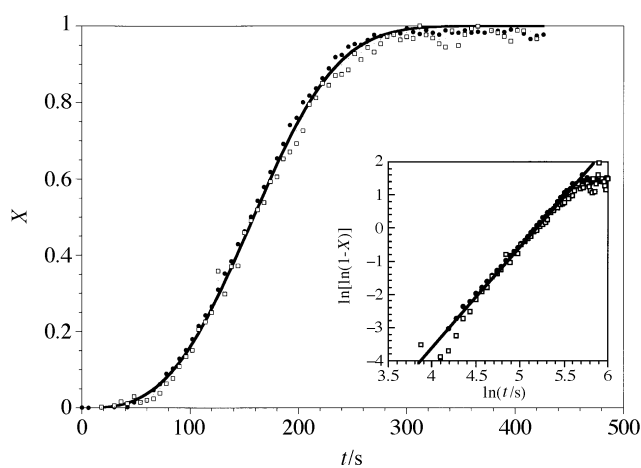


**Fig. 2** The degree of crystallinity,  $X$ , *versus* crystallisation time for PP at  $110^\circ\text{C}$ . The solid circles are SAXS and the open squares are WAXS measurements. The solid line is a fit of the Avrami equation to the average degree of crystallinity. The inset shows a conventional Avrami plot of  $[\ln(1 - X)]$  *versus*  $\ln t$ , the line has a slope of 3.

in terms of the equation

$$1 - X_s = e^{-kt^n} \quad (2)$$

where  $k$  is a rate constant and  $n$  is an integer which is sometimes interpreted in terms of the growth dimension. Fig. 2 shows a plot of  $X_s$  versus  $t$  from SAXS and WAXS in which the experimental data have been fitted with the Avrami expression over the whole of the primary crystallisation process. The fit to the data gives a value for the exponent,  $n$ , of  $3.0 \pm 0.1$  and the inset is the conventional form of the Avrami plot. The value of  $n$  obtained is consistent with random nucleation of spherulites, and is in good agreement with the crystallisation kinetics data obtained from dilatometric and calorimetric studies on iPP.<sup>25</sup> It is interesting to note that there are significant deviations of the model from the data at the extremes of crystallisation and that the evolution of the structure probed by SAXS and WAXS is also different at the beginning and end of the primary crystallisation process. The long time differences have been reviewed in some detail<sup>26</sup> whereas the initial differences have been largely ignored.

It is difficult to separate nucleation from growth in crystallisation experiments due to the low concentration of nuclei which gives rise to poor counting statistics in a scattering experiment. One potential method is to borrow from elementary chemical kinetics<sup>27</sup> and use a flow apparatus. An extruder operating at steady state provides such a set-up (see Fig. 1). Polymer above the melting point is extruded from a die, the tape or fibre cools in the air (in our case in a column of chilled nitrogen) prior to being wound up as a solid. Extrusion of tape or fibre is a steady-state process where the crystallisation time increases down the spin-line. This allowed long data collection times (minutes) for very early stages of crystallisation (milliseconds).

Prior to the development of crystals, well resolved, oriented small-angle patterns could be observed with length scales (50–200 Å) and intensities that grew down the spin-line, the corresponding WAXS showed no Bragg peaks due to crystals. Fig. 3 and 4 shows the scattering patterns collected during extrusion of iPP and HDPE. At short times these early patterns have two

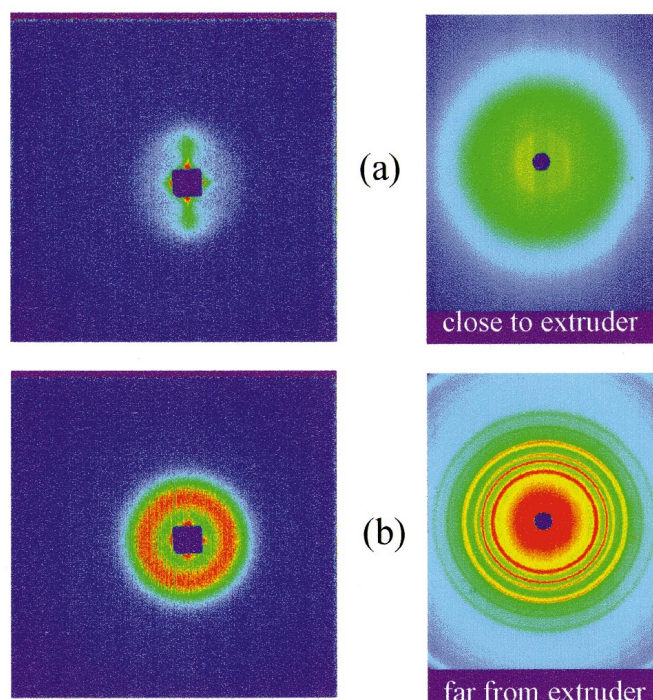


**Fig. 3** Data taken during extrusion of iPP with a low wind-up speed. 2-D wire chamber to collect the SAXS data and an image plate to collect the WAXS data. (a) Close to the die head tear shaped scattering features are observed in 2-D SAXS with only an amorphous halo in 2-D WAXS. (b) At the furthest position from the die head, when crystallisation starts, isotropic rings from crystals can be seen in SAXS and in the WAXS.

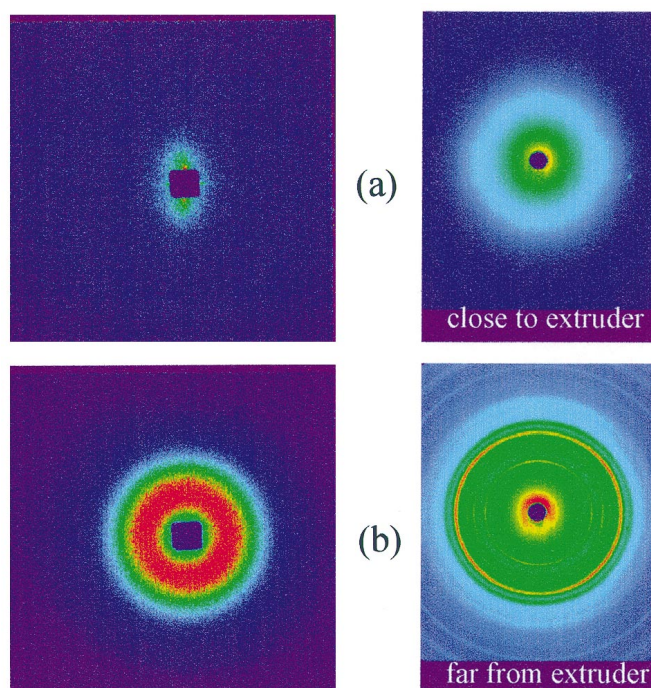


**Fig. 4** Data taken during extrusion of HDPE with a low wind-up speed. 2-D wire chamber to collect the SAXS data and an image plate to collect the WAXS data. (a) Close to the die head tear shaped scattering features are observed in 2-D SAXS with only an amorphous halo in 2-D WAXS. (b) At the furthest position from the die head, when crystallisation starts, isotropic rings from crystals can be seen in SAXS and there are oriented arcs in the WAXS (due to preferential chain orientation in the spherulites).

SAXS peaks at finite  $q$  and no WAXS peaks. We interpret this as a signature of density fluctuations. The orientation observed in the scattering is caused by coupling of density fluctuations with the slight elongational flow-field (the take-up speed was approximately twice the extrusion speed). Once crystallisation had been observed in the wide-angle region, the shape of the small-angle pattern changed from that characteristic of sinusoidal density fluctuations to that typical of lamellar crystals. Since the elongational flow was weak the crystallisation process dominated and only weakly anisotropic crystals were produced. The SAXS peaks shown at early times in Fig. 3 and 4 were approximately 100 times weaker than the diffraction ring observed in SAXS once spherulitic crystallisation had occurred.

There are a number of other possible interpretations of the data: (1) The SAXS peak could be due to the formation of oriented nuclei, the precursor to the “shish” in “shish-kebab” crystals and row nucleation,<sup>28</sup> but this should also lead to orientation in the WAXS which is not observed, furthermore, the elongation is less than a factor of 2 which is very low for formation of such structures.<sup>1,4</sup>

(2) Nucleation could have formed poorly ordered crystals which do not diffract. This would account for the lack of Bragg peaks in the WAXS (peak broadening due to small crystallites), but does not account for the peak in SAXS, the scattering from a low concentration of randomly oriented objects would give a peak at  $q = 0$  from the shape factor of the scatterers.<sup>29</sup> Guinier–Preston zones, which form in systems with conserved order parameters,<sup>30</sup> have nuclei surrounded by a depletion layer. These would give a peak in SAXS at low concentration due to the shape factor. However, in this system with a non-conserved order parameter, the nuclei are not surrounded by a depletion layer, as regions of high density grow from a background of low density with an overall increase in density, as shown in Fig. 5, and the electron density profile does not have a peak at finite  $q$ . [In crystallisation of real systems there is a non-conserved order parameter (the crystals) which is coupled to a conserved order parameter (the density).]

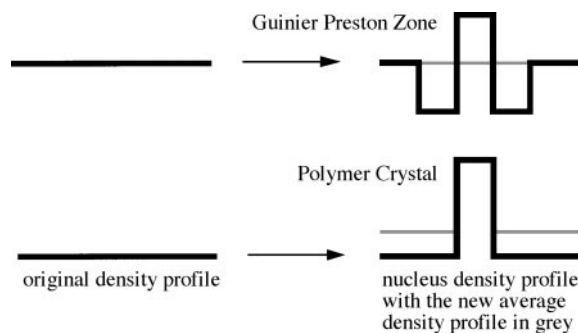


Fig. 5 Schematic diagram of the electron density profile of a Guinier–Preston zone and a nucleus for a polymer crystal.

(3) The most obvious alternative explanation of the observation is that there is an outer skin of crystalline material, due to the temperature gradient across the tape, which is giving rise to the SAXS. In this situation the crystals formed would be well ordered and one would expect them to diffract at wide angles, which is obviously not the case. Under the current experimental conditions, it is possible to observe diffraction from 1% by volume of a crystalline olefin dispersed in oil.<sup>31</sup> In order to check the temperature of the melt in the scattering volume a number of techniques were tested, an optical pyrometer indicated that the data taken close to the X-ray position [in Fig. 3(a)] had a temperature in excess of 120 °C. Whilst it is undoubtedly true that at long times crystallisation proceeds from the exterior of the tape, is unlikely that it has occurred in the data presented here.

(4) A caveat to the interpretation of the data concerns the intensity (solid angle) on the Ewald sphere. Assuming peaks of equal strength, the measured intensities scale as  $1/d^2$ , typically 100 and 5 Å for SAXS and WAXS respectively. The SAXS detector is 5 times further away from the sample so, for the same detector efficiencies, the intensities scale as the reciprocal of distance squared. Overall the measured WAXS intensity will be approximately 0.06 ( $=5^2 \times 5^2/100^2$ ) of the SAXS intensity for peaks of equal strength. For semicrystalline polymers, notwithstanding the argument above, when compared to the background intensity, WAXS peaks are generally very strong and SAXS peaks are often quite weak.

Previous SAXS/WAXS studies on polymer extrusion have concentrated on the growth and orientation of crystals.<sup>32,33</sup> Interestingly both studies, Cakmak *et al.*<sup>32</sup> on the extrusion of PVDF tape (using synchrotron radiation source and electronic detectors) and Katayama<sup>33</sup> on the extrusion of PET fibres (using a sealed tube source and film as a detector), showed SAXS before WAXS down the spin line, but made no comment on its significance.

Slow crystallisations with long induction times have been studied by simultaneous SAXS and WAXS. These experiments, on quiescent samples, show a clear development of a SAXS peak, due to electron density fluctuations, prior to the presence of crystals identified by WAXS. The peak area *versus* time data in Fig. 6 for iPP at 137 °C show, unequivocally, that the SAXS peak grows before the WAXS peak. This whole of this data set corresponds to the first 100 s in Fig. 2 and the crystallinity at 1200 s in Fig. 6 is  $\approx 0.1$ . In the first 200 s of the experiment there is no scattering above the background intensity. Between 200 and 400 s there is a measurable SAXS intensity above the background with no WAXS, after 400 s Bragg peaks are observed and after 800 s the growth in SAXS and WAXS map onto each other. The inset to Fig. 6 shows the logarithm of the peak intensity *versus* time, for the period where there is SAXS without WAXS, and it gives a good straight line fit. Similar behaviour has been reported previously for semi-rigid polymers crystallised by devitrifying a glass<sup>8–11</sup> and the kinetics of crystallisation after devitrification were analysed in terms of the Cahn–Hilliard<sup>13</sup> theory for spinodal decomposition.

It has been shown that the general form of the variation in scattered intensity,  $I(q, t)$ , following a quench is given by the following equation:

$$I(q, t) = I(q, 0)\exp[2R(q)t] \quad (3)$$

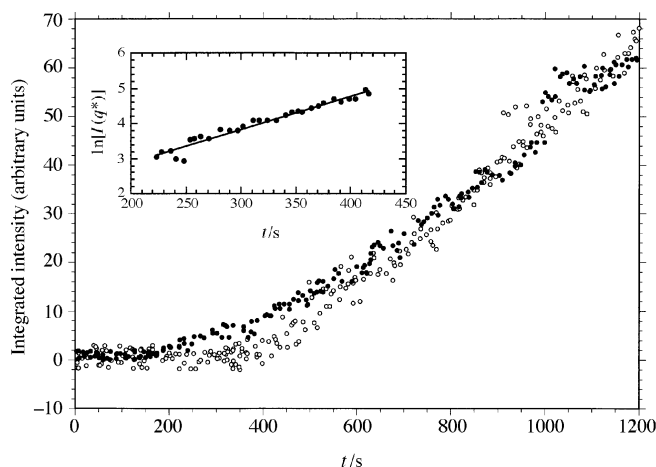


**Fig. 6** Integrated intensity data for a crystallisation at 128 °C. The open symbols are WAXS and closed symbols SAXS intensities, respectively. The inset is a plot of the logarithm of the SAXS peak intensity *versus* time.

The variation in  $I(q)$  at a given time interval is determined by the scattering law,  $P(q)$ , in the homogeneous state.  $R(q)$  is termed the growth rate constant and is given by eqn. (4)

$$R(q) = -Mq^2 \left[ \frac{\partial^2 G}{\partial \rho^2} + 2\kappa q^2 \right] \quad (4)$$

where  $M$  is the mobility term,  $G$  is the Gibbs free-energy, and  $\kappa$  is a gradient free-energy term. Modifications to eqn. (4) have been discussed previously by Cook<sup>34</sup> which take into account random thermal fluctuations (inclusion of a Brownian motion term). In employing eqn. (4) to analyse the data, the extremums are not strictly correct. The  $q$  dependence of the Onsager coefficient,  $L_0$ , relating the diffusive flux of polymer molecules to the local chemical potential has been neglected. This may be valid for the early stages of phase separation and a shallow quench. It should be noted that  $L_0$  generally does have a  $q$  dependence. This dependence has been calculated by Pincus<sup>35</sup> for a polymer blend ( $L_0 \propto q^{-2}$ ) but not for a homopolymer. Neglecting the Onsager coefficient,  $R(q)/q^2$  can be taken as a measure of the dynamic driving force for the growth of the concentration fluctuation with wave vector  $q/2\pi$ . There is a region of  $q$  in which  $R(q)$ , and thus  $R(q)/q^2$ , are positive and the concentration fluctuations do not decay but grow and give rise to phase separation. These growing concentration fluctuations have upper and lower critical boundaries to their wavenumbers. Outside these limits, the concentration fluctuations decay and do not contribute to the phase separation dynamics. As originally published, the Cahn–Hilliard theory<sup>13</sup> of spinodal decomposition is a macroscopic description and has no direct relation to events at molecular level.

The thermodynamic driving force for the growth of the concentration fluctuation with wave vector  $q/2\pi$ ,  $R(q)/q^2$ , becomes a maximum at  $q = q_m = \sqrt{G''/\kappa}$ . Thus, the wavelength,  $q/2\pi$ , of the dominant Fourier component of the growing fluctuations in the early stages of phase separation is determined by the Fourier component that exhibits maximum dynamic driving force.  $q_m$  is time independent in the early stages of phase separation and is controlled by thermodynamics.<sup>36</sup>  $R(q)$  is further controlled by the transport properties.

$$D_{\text{eff}} = -\frac{2R(q)}{q^2} \quad (5)$$

$q \rightarrow 0$

The effective diffusion coefficient,  $D_{\text{eff}}$ , can be determined from an extrapolation to  $q = 0$  of the straightline portion of  $R(q)/q^2$  during phase separation using eqn. (5) and the linearity holds for  $q_m < q < \sqrt{2}q_m$ .

Values of the amplification factor  $R(q)$ , for the early stage of crystallisation where we observe SAXS but no WAXS, were determined by plotting  $\ln I$  versus  $t$  for discrete wave vectors and finding the slope.<sup>36</sup> Fig. 7(a) shows a typical plot of  $R(q)/q^2$  versus  $q^2$ . The solid line is a fit to the data to allow estimation of  $D_{\text{eff}}$  from the  $q = 0$  intercept. The inset is a plot of  $R(q)$  versus  $q$  which shows the errors in  $R$ . Similar  $R(q)/q^2$  versus  $q^2$  plots were constructed for each polymer at a range of temperatures and those for iPP are shown in Fig. 7(b), the data have been truncated at low  $q$  as the down turn has been previously shown to be an experimental artefact.<sup>36</sup> As the crystallisation temperature is increased it should be noted that the data get less noisy (as the kinetics slow down and counting statistics improve) and the linear part of the graph is reduced, this is because  $q_m$  moves to lower values.

Fig. 8–10 show plots of  $D_{\text{eff}}$  versus  $1/T$  from which the spinodal temperature is determined by the  $D_{\text{eff}} = 0$  intercept. For example, in polypropylene at 410 K, we could estimate both the dominant length scale  $L \approx 175 \text{ \AA}$  and the effective co-operative diffusion coefficient  $D_{\text{eff}} = -4.5 \text{ \AA}^2 \text{ s}^{-1}$ . By conducting these experiments at a series of temperatures the stability limit could be found at  $415 \pm 5 \text{ K}$  (ref. 37) by extrapolation of  $D_{\text{eff}}$  to zero. The stability limits obtained in this way are compared to the melting point of an infinite crystal,  $T_m^0$ , in Table 1.

The stability limit is the temperature below which the polymer spontaneously separates into two phases. One of which is rich in polymer segments of the appropriate chain conformation to crystallise (*trans-gauche* arrangement of the carbon backbone in isotactic polypropylene, all *trans* in polyethylene<sup>38</sup>) and the other is depleted in polymer segments with the appropriate chain conformation to crystallise and is concentrated in sequences near entanglements and other defects which cannot crystallise. The stability limit is 7 K below the measured melting point for poly-

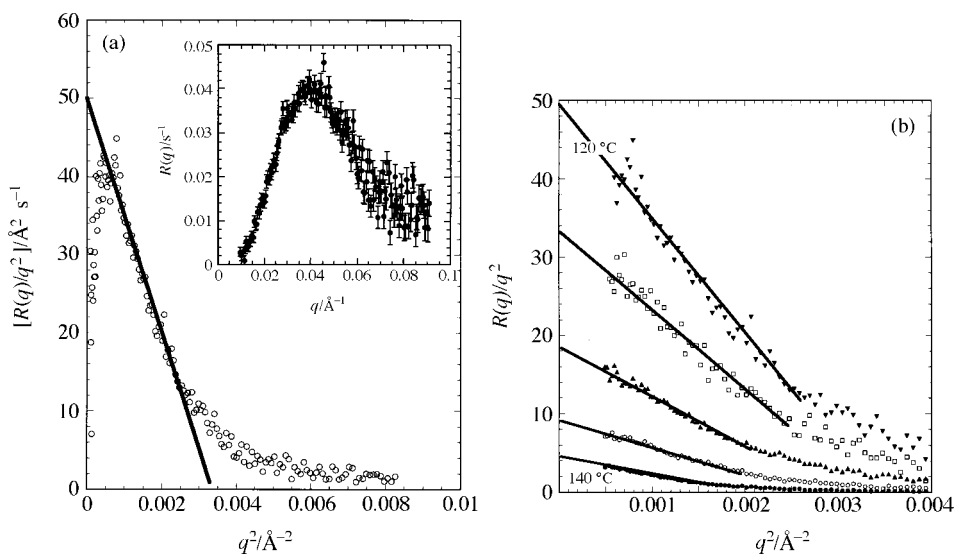


**Fig. 7** (a) Cahn–Hilliard plot to estimate the effect diffusion coefficient,  $D_{\text{eff}}$ , from the  $q = 0$  intercept of  $R(q)/q^2$  versus  $q^2$ . The solid line is a linear fit to the data. The inset shows  $R(q)$  versus  $q$  with error bars. (b) Cahn–Hilliard plots to estimate the effective diffusion coefficient,  $D_{\text{eff}}$ , for iPP at 120, 125, 130, 135 and 140 °C.

**Table 1** Stability limits and thermodynamic melting points<sup>39</sup> for the polymers studied

	$T_s$	$T_m^0$	$T_s/T_m^0$
HDPE	408	417	0.98
iPP	415	459	0.90
PET	499	573	0.87

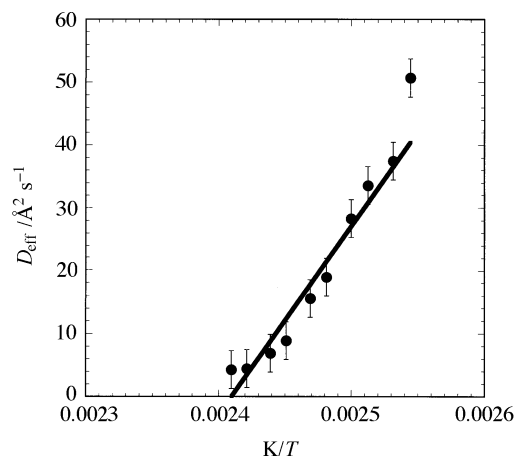


**Fig. 8** Plot of  $D_{\text{eff}}$  versus  $1/T$  (for iPP) to allow calculation of the spinodal temperature from extrapolation to  $D_{\text{eff}} = 0$ .

propylene with a long spacing of 175 Å and 44 K below the thermodynamic melting point of isotactic polypropylene.<sup>39</sup> The measured stability limits are given in Table 1. Once WAXS from crystals (atomic order on the 1 Å scale) was observed, the kinetics reverted to those of nucleation and growth, that is Avrami kinetics with an exponent  $n \approx 3$  (see Fig. 2). Similar behavior has also been observed in devitrified glasses of PET, by Kaji and co-workers,<sup>8-10</sup> and PEEK, by Ezquerra and co-workers<sup>11</sup> however, as the measurements are made close to the glass transition and the dynamics are dominated by the viscosity, estimation of the stability limit is not possible as  $D_{\text{eff}}$  increases with temperature.

For each of the polymers studied, the quiescent time-resolved SAXS/WAXS and extrusion suggest that a process that strongly resembles spinodal decomposition of chain segments with different average conformations is the nucleation step in polymer crystallisation. That polymer crystallisation occurs with phase separation is in no doubt, since at the end of the process regions of well ordered crystalline polymer coexist with regions of disordered polymer in a layered morphology (lamellae) with a spherulitic super-structure. Sequences that can be oriented with the right conformation and incorporated into the crystal separate from sequences near entanglements and

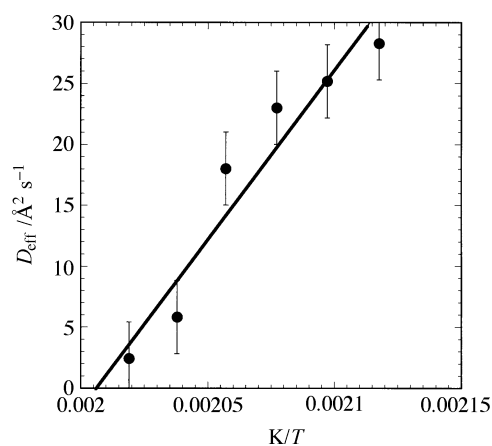


**Fig. 9** Plot of  $D_{\text{eff}}$  versus  $1/T$  (for HDPE) to allow calculation of the spinodal temperature from extrapolation to  $D_{\text{eff}} = 0$ .

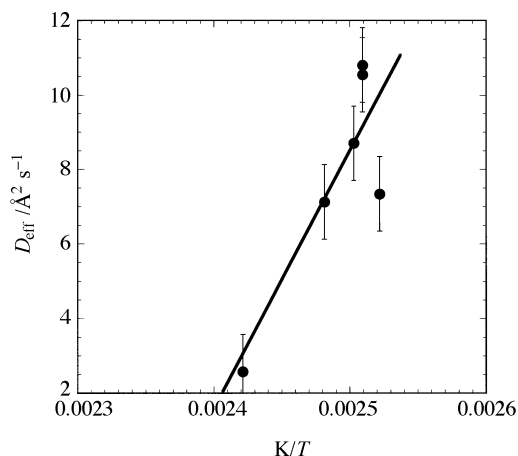


**Fig. 10** Plot of  $D_{\text{eff}}$  versus  $1/T$  (for PET) to allow calculation of the spinodal temperature from extrapolation to  $D_{\text{eff}} = 0$ .

other defects which can not crystallize and can only be part of the amorphous regions. The transformation from the disordered phase to the better ordered partially crystalline phase proceeds continuously passing through a sequence of slightly more ordered states rather than building up a crystalline state instantaneously, this is consistent with the evolution of SAXS but at some stage secondary nucleation must form crystals directly from the melt. A mechanism of continuous transformation could be consistent with a fast homogeneous nucleation process. However, it is difficult to make a clear distinction between spinodal decomposition and nucleation and growth with nucleation barriers smaller than  $k_B T$ . Polymer crystallisation, like any other phase separation, is kinetically controlled. The structure formed is the one with the highest growth rate. Once a crystallite is formed, its lateral growth rate is much higher than that of the fluctuations and so dominates. In this case the growth mechanism of semi-crystalline polymer lamellae, in the form of spherulites, takes over because the lateral growth rate of crystals (typically  $\mu\text{m s}^{-1}$ ) is  $10^4$  faster than the growth rate of the fluctuations (typically  $\text{\AA}^2 \text{s}^{-1}$ ). Thus the combination of the steady-state extrusion and the high intensity synchrotron X-ray source allows nucleation phenomena to be observed.

### Theoretical model

To understand these observations we have developed a ‘minimalist’ phenomenological model which, we believe, accurately captures the physics involved. The essential observation is the existence of spinodal-like behavior in a supercooled melt. By analogy with similar observations from metallurgy<sup>40,41</sup> and recent experiments in colloid–polymer mixtures,<sup>42</sup> as well as supercooled water,<sup>43</sup> we propose that a metastable liquid–liquid (LL) phase coexistence curve (or ‘binodal’) lies buried inside the equilibrium liquid–crystal coexistence region, as shown in Fig. 11. Quenching sufficiently below the equilibrium melting point  $T_m$ , we may cross the spinodal associated with the buried LL binodal at temperature  $T_s < T_m$ . A possible mechanism leading to such a buried LL binodal is as follows.<sup>15</sup>

In order to crystallise, polymer chains must adopt the correct conformation. For example, chains in crystalline PE have the all *trans* conformation and the chains in crystalline iPP are alternating *trans–gauche*, but in the melt the conformation is randomly *trans* or *gauche*. Generally, the preferred conformation is a helix. Furthermore, the radius of gyration of a (very long) chain changes little during crystallisation, suggesting<sup>44</sup> that neighbouring segments adopt the correct conformation and crystallise *in situ*. While it is commonly assumed that conformational and crystalline ordering occur simultaneously, we suggest that these processes can occur sequentially. Moreover, chains with different conformations have different densities, and therefore also different

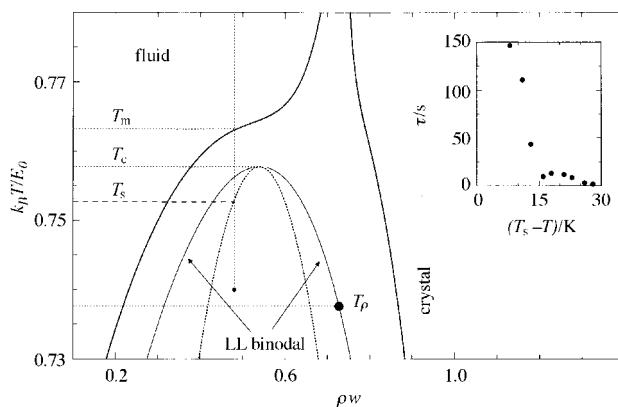


**Fig. 11** Proposed generic phase diagram for a polymer melt with a buried liquid–liquid phase predicted by the SAC model.<sup>15</sup>  $T_m$  and  $T_s$  are the melting and spinodal temperatures encountered along the constant density quench path (dotted line). Inset shows the measured induction time as a function of temperature for iPP.

energy barriers for reorientation between rotational isomeric states (RIS).<sup>45</sup> Such conformation–density coupling can induce a LL phase transition. A phenomenological free energy which incorporates these effects is a function of the mean mass density  $\bar{\rho}$ , the coefficients of the Fourier expansion of the crystal density in the reciprocal lattice vectors (essentially the intensities of Bragg peaks), and the relative occupancies of various RIS. Consider a free energy with a single Fourier mode  $\rho_*$  (corresponding to BCC symmetry<sup>46</sup>) and a pair of RIS, with  $\eta$  the population of the ground (*trans*) state:

$$f = f_0(\bar{\rho}) + f_*(\bar{\rho}, \rho_*) + f_\eta(\eta, \bar{\rho}, \rho_*) \quad (6)$$

The first term,  $f_0$ , is the free energy of a melt with random chain conformations.<sup>47</sup> The (bare) Landau free energy of crystallisation is given by  $f_*(\bar{\rho}, \rho_*)$ .  $f_\eta$  describes how the distribution of chain conformations varies smoothly from a random coil ( $\eta = 0$ ) to a helix ( $\eta = 1$ ) as the temperature is lowered.<sup>48</sup> In isolation, a polymer thermally populates its RIS with a Boltzmann distribution; to incorporate the coupling between density and conformation, we take the energy gap to have the phenomenological form

$$E(\bar{\rho}, \rho_*) = E_0 + v\bar{\rho} + \lambda\rho_*^2 \quad (7)$$

As more bond sequences occupy the ground state, monomers can rearrange to pack tighter and reduce the excluded volume interaction (hence the perturbation  $v\bar{\rho}$ ). A positive  $v$  encourages phase separation to take advantage of this density–conformation coupling. Similarly, adjacent ground state sequences enhance crystallisation (hence the term  $\lambda\rho_*^2$ ). The  $\lambda$  term is quadratic in  $\rho_*$  by symmetry.<sup>46</sup> To calculate the phase diagram we must minimize the free energy over the mean polymer conformation, and then compare the free energy of amorphous and crystal branches of the free energy, finally using the common tangent construction to find the equilibrium state.

Physically, this calculation says that at low enough temperatures, the system gives up conformational entropy to relieve packing frustration, and separates into a dense, more conformationally homogeneous liquid and a less dense and more conformationally disordered liquid. In practice, this happens only at appreciable rates by spinodal decomposition, giving rise to two coexisting liquids, with a coarsening interconnected domain texture, as shown in Fig. 12. The dense liquid is closer in density and conformation to the crystal phase than the original melt, with a lower energy barrier  $\Delta$  to crystallisation. We expect  $\Delta$  to decrease with increasing quench depth below  $T_s$ . The induction time  $\tau_i$  is then a sum of the time to coarsen into an intermediate spinodal texture, and an exponential activation time determined by  $\Delta$ . The strong temperature dependence of  $\tau_i$  should change over to a much weaker dependence at some  $T_\rho < T_s$ , where  $\Delta(T_\rho, \bar{\rho}) \leq k_B T_\rho$ . This has been found in iPP (inset, Fig. 11).<sup>12</sup>

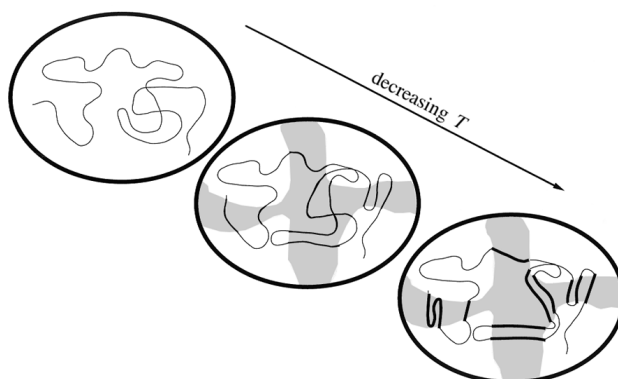


**Fig. 12** Schematic diagram illustrating the continuous transformation from a Gaussian chain, through a microphase separated liquid to a semi-crystalline polymer. Coexisting liquid phases with different conformations, showing a single chain; thin line = disordered conformation, thick line = correct (helical) conformation for crystallisation. Each chain is a ‘conformational copolymer’.

Our arguments so far have been based on conformation-density coupling. An analogous argument may be made in terms of a liquid–crystalline coupling, by which density-orientation effects become more important as the polymer stiffens upon cooling into the preferred helical conformation. This approach was adopted by Imai and co-workers,<sup>10</sup> and probed by light scattering. Indeed, the two mechanisms have, in the main, the same physical content.

Until recently, spinodal scattering was mainly observed in polymer melts crystallising under shear.<sup>7,32,49</sup> This may be understood in a natural way within the present framework. Shear (and extensional) flow couples principally to the orientation of polymer segments, hence straightening chains and enhancing  $\eta$ , thereby biasing the tendency towards LL separation. A simple way to incorporate this is to renormalise the activation energy  $E$  as  $E - v_0 \sigma$  where  $\sigma$  is the stress. It is highly suggestive that, for appropriate values of stress under strong flow (the plateau modulus  $G_0$ ) and volume ( $v_0$  above), the LL binodal of Fig. 11 is shifted upward significantly (by  $\delta T_s \sim 0.01E_0/k_B$ ). Flow will shift the liquid–solid coexistence curve much less because the regions with crystalline order will resist deformation. This simple theory suggests several interesting experiments. First, conformational fluctuations just above  $T_g$  could be detected and studied, *e.g.* by Raman spectroscopy,<sup>7</sup> perhaps simultaneously with depolarised light scattering (to monitor orientational fluctuations). Second, upon approaching a spinodal line various properties (*e.g.* correlation length) should exhibit power-law divergences. Third, the LL spinodal line can be modified by pressure. In particular, it may be possible to access the LL critical point,  $T_c$ : recent simulations suggest a massive enhancement of the nucleation rate in the vicinity of  $T_c$ .<sup>50</sup> The effect of strain on the crystallisation of PET close to the  $T_g$  has been studied, using elegant time resolved scattering experiments, by Blundell *et al.*<sup>51</sup> Crystallisation (determined by WAXS) occurred after the extension of 4 : 1 and followed first order kinetics (*i.e.* Avrami  $n = 1$  which is equivalent to spinodal). Close to the  $T_g$  the rate of the transformation was temperature insensitive as a reduction in temperature caused an increase in the dynamic driving force but a reduction in mobility. These authors interpret this data as the LL energy barrier being reduced by chain orientation in extensional flow.

More generally, the coupling of density to (molecular) structural order parameters is an emerging generic theme in the study of supercooled liquids (water–amorphous ice;<sup>43</sup> polymer melts near the glass transition<sup>52</sup>). Balsara and co-workers<sup>53</sup> have described interesting behaviour in hexagonal rod forming block copolymers subjected to a deep quench. The microstructure formation in the liquid and crystal directions is not correlated, the growth of crystalline order occurs before the development of a coherent structure along the liquid direction and they argue that this may be a signal of spinodal decomposition in liquid crystals. The ratio of  $T_g/T_m$  observed is 0.977 which is in the range described here for polymer crystallisation. The analogy for the case presented here would be chains pack locally, in straight sections, prior to becoming oriented along their length into lamellae.

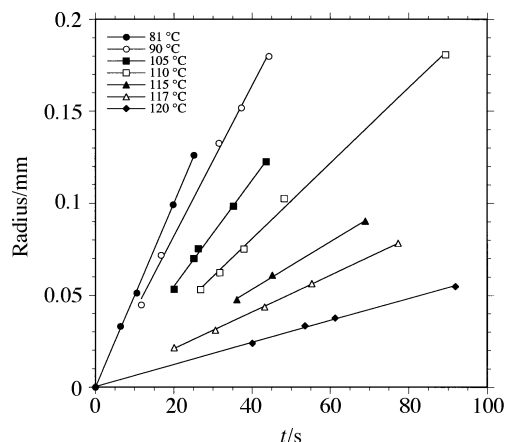


Fig. 13 Data from Ratajski and Janeschitz-Kriegl<sup>17</sup> showing that a plot of spherulite radius *versus* time passes through the origin for a wide range of crystallisation temperatures in iPP.

## Discussion

It is obviously very difficult to make a clear distinction between spinodal decomposition and nucleation and growth with nucleation barriers smaller than  $k_B T$ . Crystallisations with long induction times, studied by small and wide angle X-ray scattering (SAXS and WAXS), reveal the onset of large scale ordering prior to crystal growth. Rapid crystallisations studied by melt extrusion indicate the development of well resolved oriented SAXS patterns associated with large scale order before the development of crystalline peaks in the WAXS region. The results suggest pre-nucleation density fluctuations play an integral role in polymer crystallisation.

An interesting observation is made by Ratajski *et al.*<sup>17</sup> Extrapolated spherulite size curves for temperatures below  $T_p$  show no induction time, that is the line through the radius *versus* time curve (Fig. 13) passes through the origin despite the fact that X-ray, heat and density measurements show a clear induction time (see Fig. 2). Recent rheological studies<sup>16</sup> show that gelation occurs in crystallising melts at very low degrees of crystallinity, typically <3%, shortly after  $\tau_i$ . This means that there is a percolating network formed that is observed in the dynamic mechanical response of the system. Both pieces of evidence indicating large-scale structure is formed prior to the appearance of Bragg peaks or evolution of appreciable enthalpy. It is tempting to consider setting up an instantaneous structure that in the conformation and density that comprises isotropic sine waves with random phase and direction but fixed wavelength. This sets the subsequent lamellar thickness or long spacing. The crystallisation process which forms the perfected crystals which show Bragg peaks is a perfection and formation of grains, the growth of which we see as spherulites.

In a technical context, Galilietner and co-workers have shown<sup>54</sup> that nucleating agents are most effective in the "metastable supercooling zone". Nucleating agents cease to work in iPP at around 140 °C which is close to the measured  $T_s$  and that homogeneous nucleation takes over at temperatures below 110 °C which is close to  $T_p$ . This is in general agreement with our theoretical model and experimental results, the crystallisation rate is vanishing above  $T_s$  and homogeneous nucleation is very fast below  $T_p$ .

## Acknowledgements

The experimental work originated from an EPSRC ROPA to Professor R. J. Young and A.J.R. at UMIST. W.C.K. and P.D.O. started the theoretical work whilst W.C.K.P. was on sabbatical in Leeds. The many heated discussions with, and constructive criticism from, Tom Mcleish, Frank Bates, Herve Marand, Andrew Keller, Paul Phillips, Gerhard Eder, Julia Higgins and John Blackwell are most appreciated.

## References

- 1 A. N. Wilkinson and A. J. Ryan, *Polymer Processing and Structure Development*, Kluwer, Amsterdam, 1998.
- 2 (a) J. I. Lauritzen and J. D. Hoffman, *J. Res. Natl. Bur. Stand. Sect. A*, 1960, **64**, 73; (b) J. D. Hoffman, J. I. Lauritzen, E. Passaglia, G. S. Ross, L. J. Frohler and J. J. Weeks, *Kolloid. Z. Poly.*, 1969, **231**, 564; (c) J. D. Hoffman, G. T. Davis and J. I. Lauritzen, *Treatise on Solid State Chemistry*, Plenum, New York, 1976; (d) J. Petermann, R. M. Gohil, J. M. Schultz, R. W. Hendricks and J. S. Lin, *J. Polym. Sci. Polym. Phys. Edn.*, 1982, **20**, 523; (e) D. M. Sadler, *Polym. Commun.*, 1986, **27**, 140; (f) D. M. Sadler, *Polymer*, 1987, **28**, 1440.
- 3 R. J. Young and P. A. Lovell, *Introduction to Polymers*, Chapman and Hall, London, 2nd edn., 1991.
- 4 See, for example, A. Keller and H. W. H. Kolnaar, in *Materials Science and Technology*, ed. R. W. Cahn, P. Haasen and E. J. Kramer, Wiley-VCH, Weinheim, 1997, vol. 18, ed. H. E. H. Meijer; P. Barham, in *Materials Science and Technology*, ed. R. W. Cahn, P. Haasen and E. J. Kramer, Wiley-VCH, Weinheim, 1993, vol. 12, ed. E. L. Thomas.
- 5 G. Eder and H. Janeschitz-Kriegl, in *Materials Science and Technology*, ed. R. W. Cahn, P. Haasen and E. J. Kramer, Wiley-VCH, Weinheim, 1997, vol.18, ed. H. E. H. Meijer.
- 6 D. C. Bassett, *Principles of Polymer Morphology*, Cambridge University Press, Cambridge, 1981.
- 7 G. Strobl, *The Physics of Polymers*, Springer-Verlag, Berlin, 1996.
- 8 M. Imai, K. Kaji, T. Kanaya and Y. Sakai, *Phys. Rev. B*, 1995, **52**, 12696.
- 9 M. Imai, K. Mori, T. Mizukami, K. Kaji and T. Kanaya, *Polymer*, 1992, **33**, 4451; *ibid*, 1992, **33**, 4457.
- 10 M. Imai, K. Kaji and T. Kanaya, *Macromolecules*, 1994, **27**, 7103.
- 11 T. A. Ezquerra, E. López-Cabarcos, B. S. Hsiao and F. J. Baltà-Calleja, *Phys. Rev. E*, 1996, **54**, 989.
- 12 N. J. Terrill, J. P. A. Fairclough, E. Towns-Andrews, B. U. Komanschek, R. J. Young and A. J. Ryan, *Polymer*, 1998, **39**, 2381.
- 13 J. W. Cahn and J. E. Hilliard, *J. Chem. Phys.*, 1958, **28**, 25; J. D. Gunton, M. San Miguel and P. S. Sahni, in *Phase Transitions and Critical Phenomena*, ed. C. Domb and M. S. Green, Academic, New York, 1983, vol. 8.
- 14 H. Janeschitz-Kriegl, *Colloid Polym. Sci.*, 1997, **81**, 1121.
- 15 P. D. Olmsted, W. C. K. Poon, T. C. B. McLeish, N. J. Terrill and A. J. Ryan, *Phys. Rev. Lett.*, 1998, **81**, 373.
- 16 N. V. Pogodina and H. H. Winter, *Macromolecules*, 1998, **31**, 7103.
- 17 E. Ratajski and H. Janeschitz-Kriegl, *Colloid Polym. Sci.*, 1996, **274**, 938.
- 18 I. W. Hamley, J. P. Fairclough, N. J. Terrill, A. J. Ryan, P. Lipic, F. S. Bates and E. Towns-Andrews, *Macromolecules*, 1996, **29**, 8835.
- 19 W. Bras and A. J. Ryan, *Adv. Colloid Interface Sci.*, 1998, **75**, 1.
- 20 W. Bras, G. E. Derbyshire, J. Cooke, B. E. Komanschek, A. Devine, S. M. Clark and A. J. Ryan, *J. Appl. Cryst.*, 1994, **28**, 26.
- 21 <http://www.dl.ac.uk/SRS/NCD/manual.otoko.html>
- 22 I. W. Hamley, R. C. Denny, M. Matsen, B. Liao, C. Booth and A. J. Ryan, *Macromolecules*, 1997, **38**, 509; <http://wserv1.dl.ac.uk:800/SRS/CCP13/program/fit.html>
- 23 A. J. Ryan, J. L. Stanford, W. Bras and T. M. W. Nye, *Polymer*, 1997, **38**, 759.
- 24 M. Avrami, *J. Chem. Phys.*, 1939, **7**, 1103; *ibid*, 1940, **8**, 212; *ibid*, 1941, **9**, 177; L. Marker, F. M. Hay, G. P. Tilley, *J. Polym. Sci.*, 1959, **38**, 107.
- 25 *Polypropylene*, ed. J. Karger-Kocsis, Chapman & Hall, London, 1995, vol. 1.
- 26 R. K. Verma and B. S. Hsiao, *Trends In Polymer Science*, 1996, **4**, 312; B. S. Hsiao, B. B. Sauer, R. K. Verma, H. G. Zachmann, S. Seifert, B. Chu and P. Harney, *Macromolecules*, 1995, **28**, 6931; M. Bark and H. G. Zachman, *Acta Polymerica*, 1993, **44**, 259.
- 27 P. W. Atkins, *Physical Chemistry*, OUP, Oxford, 6th edn., 1997.
- 28 A. Keller and F. M. Willmouth, *J. Macromol. Sci.*, 1972, **B6**, 493.
- 29 O. Glatter and O. Kratky, *Small Angle X-ray Scattering*, Academic Press, NY, 1982.
- 30 A. Guinier and G. Fournet, *Small Angle Scattering of X-rays*, Chapman & Hall, London, 1955.
- 31 B. Hsiao, personal communication.
- 32 M. Cakmak, A. Teitge, H. G. Zachmann and J. L. White, *J. Polym. Sci. Polym. Phys. Edn.*, 1993, **31**, 371.
- 33 K. Katayama, *Kolloid Z. Z. Polym.*, 1968, **226**, 125.
- 34 H. E. Cook, *Acta Metall.*, 1970, **18**, 297.
- 35 P. Pincus, *J. Chem. Phys.*, 1981, **75**, 1996.
- 36 F. S. Bates and P. Wiltzius, *J. Chem. Phys.*, 1989, **91**, 3258.
- 37 K. Binder in *Materials Science and Technology*, ed. R. W. Cahn, P. Haasen and E. J. Kramer, Wiley-VCH, Weinheim, 1993, vol. 5, ed. P. Haasen.
- 38 H. Tadokoro, *Structure of Crystalline Polymers*, John Wiley & Son, 1979.
- 39 J. E. Mark, *Physical properties of Polymers*, American Institute of Physics, NY, 1996.
- 40 J. W. Cahn, *Trans. Metall. Soc. AIME*, 1968, **242**, 166.
- 41 See, J. W. Martin, R. D. Doherty and B. Cantor, *Stability of microstructures in metallic systems*, Cambridge University Press, Cambridge, 1997.

- 42 W. C. K. Poon, A. D. Pine and P. N. Pusey, *Faraday Discuss.*, 1995, **101**, 65; M. R. L. Evans, W. C. K. Poon and M. E. Cates, *Europhys. Lett.*, 1997, **38**, 595.
- 43 S. Harrington, R. Zhang, P. H. Poole, F. Sciortino and H. E. Stanley, *Phys. Rev. Lett.*, 1997, **78**, 2409.
- 44 M. Dettenmaier, E. W. Fischer and M. Stamm, *Colloid Polymer Sci.*, 1980, **258**, 343.
- 45 L. R. Pratt, C. S. Hsu and D. Chandler, *J. Chem. Phys.*, 1978, **68**, 4202.
- 46 S. Alexander and J. McTague, *Phys. Rev. Lett.*, 1978, **41**, 702.
- 47 J. Brandrup and E. H. Immergut, *Polymer Handbook*, Wiley, NY, 3rd edn., 1989.
- 48 P. J. Flory, *Statistical Mechanics of Chain Molecules*, Oxford University Press, Oxford, 1989.
- 49 *Flow-induced Crystallization in Polymers Systems*, ed. R. L. Miller, Gordon and Breach, NY, 1979.
- 50 P. R. ten Wolde and D. Frenkel, *Science*, 1997, **277**, 1975.
- 51 D. J. Blundell, D. H. McKerron, W. Fuller, A. Mahendrasingham, C. Martin, R. J. Oldman, R. J. Rule and C. Riekell, *Polymer*, 1996, **37**, 3303.
- 52 T. Kanaya, A. Patkowski, E. W. Fischer, J. Seils, H. Glaser and K. Kaji, *Acta Polym.*, 1994, **45**, 137.
- 53 N. P. Balsara, B. A. Garetz, M. C. Newstein, B. J. Bauer and T. J. Prosa, *Macromolecules*, 1998, **31**, 7668.
- 54 M. Gahleitner, J. Wolfschwenger, C. Bachner, K. Bernreitner, W. Neissl, *J. Appl. Polym. Sci.*, 1996, **61**, 649.

Paper 9/00246D